

Characterisation of 3D woven textile composites in presence of minor weft tow undulations and cross-section variations

Mingming Xu^{1,2}, Elena Sitnikova^{1*}, Weiyi Kong³, Jian Zhang⁴, Shoufeng Hu⁴ and Shuguang Li¹

¹Faculty of Engineering, University of Nottingham, Nottingham, NG8 1BB, UK

²School of Science, Harbin Institute of Technology (Shenzhen), Shenzhen, 518055, P. R. China

³TaiHang Laboratory, No. 619, Jicui Street, Tianfu New Area, Chengdu, Sichuan Province, 610213, P. R. China

⁴AECC Commercial Aircraft Engine CO., Ltd, Shanghai 200241, P.R. China

*Corresponding author elena.sitnikova@nottingham.ac.uk

Abstract: Weft tows in 3D woven composites are commonly approximated as perfectly straight, but their undulations are inevitable in reality, although the extent of undulations in the weft tows is not as pronounced as in the warp tows. Such minor undulations in weft tows have been simulated in this paper. A previously established parametrised modelling and analysis tool for 3D woven composites has been extended to reproduce the varying geometry of the weft tows. Two novel models have been proposed to introduce the undulations, allowing their effects to be simulated. The analysis reveals that, compared to the model with straight weft tows, the effective elastic properties can be affected by the weft tow undulations. In addition, the procedure for defining varying intra-tow fibre orientation was formulated and implemented, addressing lack of consistent and robust functionalities of this kind in modern finite element solvers.

Keywords: 3-Dimensional reinforcement; Elastic characterisation; Material orientation; Undulation

1 Introduction

The subject of 3D woven textile composites is being actively researched at present. The major advantage of the woven composites compared to conventional laminates is their integral construction [1]. This substantially improves their structural integrity under transverse loadings, such as impact [2]. One of the major challenges in numerical characterisation of these

materials is how to represent the internal structure of the tows in the textile reinforcement in the models.

Various methods of modelling and characterisation of woven composites have been reported in the literature. During the 1990s, the simplest geometric modelling method of the woven preforms, called the fibre inclination model, was proposed to construct the idealised unit cell (UC) based on the orientation of the fibre bundles [3, 4], in which the fibre yarns were idealised as straight beams. Later, by using computer-aided geometric design techniques, an improved approach to a structural representation of woven architectures was developed in both parametric and graphic forms [5-7]. Its basic idea is to create each yarn in the preform by sweeping a closed profile along a centreline path [6]. This procedure for the generation of woven models has been implemented as weave modelling software, best known of which are WiseTex [8] and TexGen [9].

This geometry modelling technique is employed typically for generating the geometry of the unit cell models representing the woven textile composites. Unit cell modelling is a popular method for mechanical characterisation of woven composites [10-12]. This type of analysis is often carried out using finite element solvers, where the otherwise demanding material characterisation procedures can be highly automated, as it was done in a UnitCells© tool [13]. Unit cell modelling of the 2D and 3D woven composites typically involves idealisation, where the shape and the size of the cross-sections are assumed to remain constant along the paths of the respective tows [11, 14]. The geometric dimensions of the tow cross-section are measured directly from micro-computed tomography (micro-CT) images [15, 16]. The statistical mean value of the geometric parameters ensures a certain accuracy of these measurements in terms of representing the weave geometry. It has been argued in [17] the direct measurements of the geometry can be very subjective, even after some statistical processing, because there is no standard verified methodology for conducting such measurements. As an efficient alternative to direct measurement of geometric parameters, a procedure was established in [17] where they are calculated directly from the manufacturing ones. This procedure is universally applicable to 3D woven composites based on layer-to-layer angle interlock reinforcement, and it eliminates subjectivity in geometry definition to a great extent.

The main criticism of the analysis techniques based on the idealised UC models is the insufficient accuracy of predictions of the effective properties of woven composites, which is believed to be primarily associated with lack of representation of geometric variability in woven reinforcements. As an attempt to improve the prediction accuracy, the micro-CT-based modelling of textile composites started to gain popularity over the past decade [18-23]. The

main underlying consideration is that the geometrical models that incorporate numerous varying features of the woven reinforcement should produce a closer representation of the actual material and hence would deliver closer agreement with the experiment than the idealised models that do not comprise such geometric variations.

While the highly detailed geometric models are indeed reported to offer improvement in terms of the agreement with the experimental data, the relative difference between the predictions delivered by them and those obtained with the idealised ones is not overwhelming, typically within a few percent, especially for the elastic characterisation results. Besides, such improvement in agreement with an experiment does not necessarily indicate a superior predictive capability. Specifically, sophisticated geometric models usually require multiple parameters, measurement procedures for which are not established. Definition of those would inevitably involve carrying out some calibrations and introduction of further assumptions to achieve close agreement with the experimental data. Whether the same procedures and assumptions would deliver the same accuracy of predictions if different material systems were used and the overall geometry, such as the tow sizes, was changed, is still an open question. Therefore, it is too early to dismiss the idealised model on the basis on low accuracy of predictions, at least as far as the elastic characterisation is concerned. On the other hand, when damage and strength characterisation are involved, due representation of localised geometric features can indeed play an important part, as those can act as stress concentrators.

It is also worth noting that the material characterisation techniques involving the geometric models with variability as cited above have been developed and applied to 3D woven composites of a particular type, namely, the orthogonal interlock, in which the binder yarns interlace the layers of straight weft and warp tows through the thickness of the fabric. For them, variation of the tow cross-sections shapes through the thickness can be quite significant. Furthermore, the unit cells for such materials would have to incorporate the surface layers, where the fibre tows typically undergo a substantial compaction. Therefore, for this type of 3D woven composites, modelling of localised features of the woven architecture can be a necessity for adequate representation of the woven reinforcement geometry.

On the other hand, internal architecture of 3D woven composites based on layer-to-layer angle interlock reinforcement is sufficiently regular to allow representation by a unit cell comprising one weft and one warp tow in the thickness direction [11]. Such unit cell represents the 3D woven architecture discounting the surface layers, the geometric and topological constructions of which are different from those of the layers within the weave [17]. The architecture of such UC has been fully parametrised by seven geometric and five topological

parameters [11] and due to its reasonably small size, it is computationally efficient. These factors make it a highly useful analysis tool in composites design exercises. It is obvious that the highly detailed geometric models are unsuitable for use in design due to lack of practical parametrisations and their low computational efficiency. At the same time, when idealising the woven architecture to produce a unit cell, many varying geometric features are neglected, as is the common practice in such idealisations. Given general lack of justifications for doing so in the open literature, typical variabilities in the 3D layer-to-layer angle interlock composites are reviewed in the next section, where they are classified into two categories, random and periodic.

It is the effects of periodic variability which primarily show as undulations in the weft tows that will be the subject of this paper. Instead of maximising the complexity of the model and assessing the joint contribution of numerous varying geometric features as in the detailed geometric models reviewed above, conceptually different approach to modelling the varying geometry was taken, where a typical varying feature has been isolated and its effect on the mechanical behaviour of the woven composite has been exposed. The rationale behind that is that when numerous varying geometric features are present, one cannot reliably judge which ones have the most significant effect on the results and which have only a marginal influence. It is lot easier to make such judgement when such features are considered individually. Equally important consideration is that it would allow to retain the UC as the analysis tools. The previously established idealised UC [11] will be supplemented with capability to incorporate the periodic variations of the cross-sections of the weft tows along their paths by parametrising the latter. Having established a systematic and efficient capability for incorporating such periodic variation in the UC model, one can readily employ when carrying out the characterisation exercises, or can include it as an additional consideration when coming up with a design of the woven reinforcement.

2 Typical varying geometric features in woven textile preforms

2.1 Types of varying geometric features of the woven architecture

The varying geometric features in woven textile composites can be divided into two general categories: the random and the periodic ones. The former one comprises features that are not repeated consistently in the weave and therefore cannot be represented in the unit cell. Typical examples are the defects (voids) in the matrix due to imperfect impregnation [24]. To reproduce such features in an FE model, a sufficiently large patch of the material would have

to be considered in which all possible variability could be duly incorporated. This would be extremely time-consuming and one would also have to rely on the availability of the experimental facilities [22, 25], like high-resolution X-ray scanners, image processing and statistical analysis tools [26]. Such variability will not be addressed in this paper.

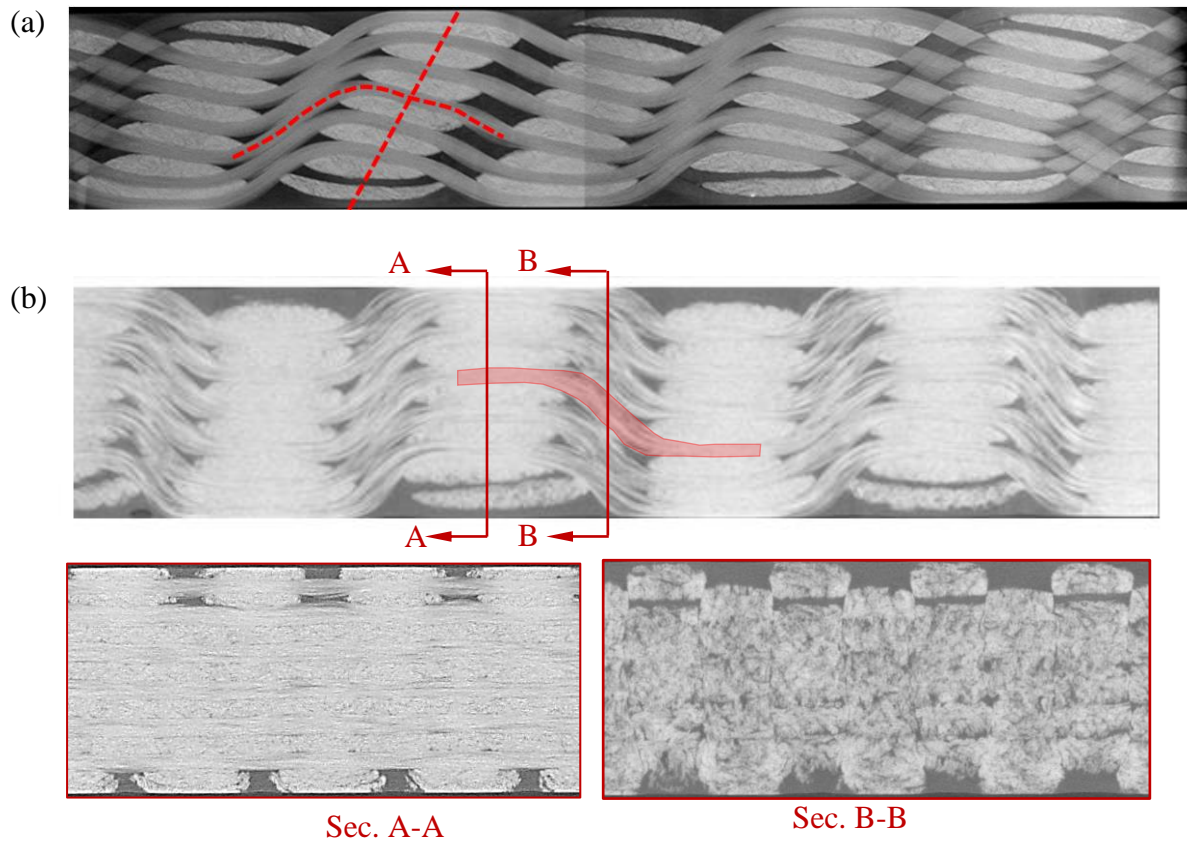


Fig. 1 Examples of varying geometric features in 3D woven composites [27]: (a) T300 carbon fibre woven reinforcement, (b) E-glass fibre woven reinforcement

Examples of the periodic variations of the reinforcement geometry are shown in Fig. 1, where the micro-CT images of cross-sections of the carbon and the glass fibre 3D woven composites [27] are presented. The cross-sections have been taken orthogonally to the direction of the weft tows. The weft tows are straight, and they are regularly arranged in rows and columns within the weave. The undulating warp tows interlace the weft ones. A variable feature shown in Fig. 1(a) is tilting and curving of straight columns of weft tows in the fabric as a result of compaction by the mould tool during the resin transfer moulding (RTM) forming. Another example of a periodic variable feature is swelling of the warp tows in the direction transverse to the tow between the columns of the weft tows due to lack of transverse constraint. This tendency is illustrated in Fig. 1(b). Specifically, the strongest compaction of warp tows is

shown in cross-sectional view A-A in Fig. 1, where section is taken along the middle of the weft tow column. On the other hand, cross-sectional view B-B demonstrates that the swollen warp tows have taken up the cavity between the neighbouring warp tows, while their width effectively remains the same. Note that the warp tows in the surface layers of the composite also experience sideways expansion in section A-A due to lack of sideways constraint. However, surface layer effects will not be addressed in the present paper.

In contrast to the random variability features, the periodic variable features can be effectively represented in a unit cell to reveal and assess their effect on the mechanical performance of textile composites. Note that some features of reinforcement, while periodic, do not systematically occur in the woven composites, such as tilting of the columns of the weft tows as shown in Fig. 1(a). It occurred due to rough handling of the preform prior to moulding and is therefore not consistently reproduced in woven composites. This undesirable feature should not be confused with the weave configuration where shift of the weft layers is a designed feature of the reinforcement, implemented during weaving of the preform. There are means of incorporating such shift in the model, for example, using a readily available functionality in Wisetex tool [28, 29].

On the other hand, any periodically repeating variation of the weave architecture that systematically occurs in a wide range of composites requires relevant investigation. An appropriate decision should be made whether a feature should be kept in the model due to its substantial influence of the mechanical properties, or whether it can safely be neglected otherwise. A variable feature of this kind that has never been examined systematically is the periodic variation of the weft cross-sections and the minor undulations along the weft tow path. Such undulations differ fundamentally from those in the warp tows, because the latter were intended while the former were not. Therefore, it is neither reasonable nor efficient to treat them in the same way. A comprehensive description of such minor undulations is given in the subsection below. Its practical representation in the unit cell will be established, and its influence on the mechanical performance of the composite will be assessed.

2.2 Variations of the weft tow cross-section

The variations in the geometry of the weft tow were identified by visually inspecting the images of cross-sections of woven composites obtained with the micro-CT. The composite considered here was of 3D woven layer-to-layer angle interlock architecture, idealised model of which is shown in Fig. 2. In this figure, the typical planes of cross-sections where the most distinctive geometric features of the weft tows can be observed have also been marked.

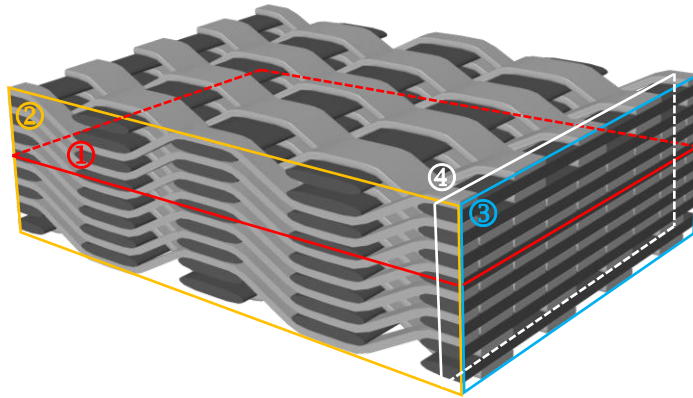


Fig. 2 Model of 3D woven layer-to-layer angle interlock reinforcement

The inspection of cross-sections reveals that when viewed from the top, the weft tows remain reasonably straight and retain constant width along their paths, as can be seen in Fig. 3(a). However, when considering weft tow cross-section profiles in Fig. 3(b), systematic variation in their shape can be observed. Specifically, when the warp tow undulates over the weft tow, the right and left sides of the weft tow cross-section are shifted downwards; similarly, when the warp tow undulates under the weft tows, the right and left sides of the weft cross-section are moved upwards. This unbalanced compaction from the warp tow tends to shape the cross-section of weft tows such that it can be idealised by two half-ellipses with one half flattened more than the other, depending on the side the warp tow undulating around it. Outlines of such modified cross-section profiles are marked in red in Fig. 3(b).

The undulations in the weft tows can be observed as follows. When the cross-section is taken through the centre of the weft tows, as marked by plane ③ in Fig. 2, the cross-sections of the weft tows are reasonably straight, as can be seen Fig. 3(c-1). However, for cross-sections taken closer to the sides of the weft tow, such as that marked by plane ④ in Fig. 2, the weft tow undulations are apparent, as can be clearly seen in Fig. 3(c-2), where the directions of undulation are marked by arrows. This is due to alternating compaction from the adjacent warp tows that wrap around the weft tow on the opposite sides. At the borderline between the two neighbouring warp tows, marked by a red line in Fig. 3(a), the weft tow cross-sections are subjected to equal compaction from both sides and its profile is not biased and can be represented by an ellipse as shown inset to Fig. 3(a).

Such minor variation of the weft tow is a typical feature of layer-to-layer angle interlock architectures. In particular, localised undulations of the weft tows can also be observed in micro-CT images of carbon fibre composite shown in Fig. 4.

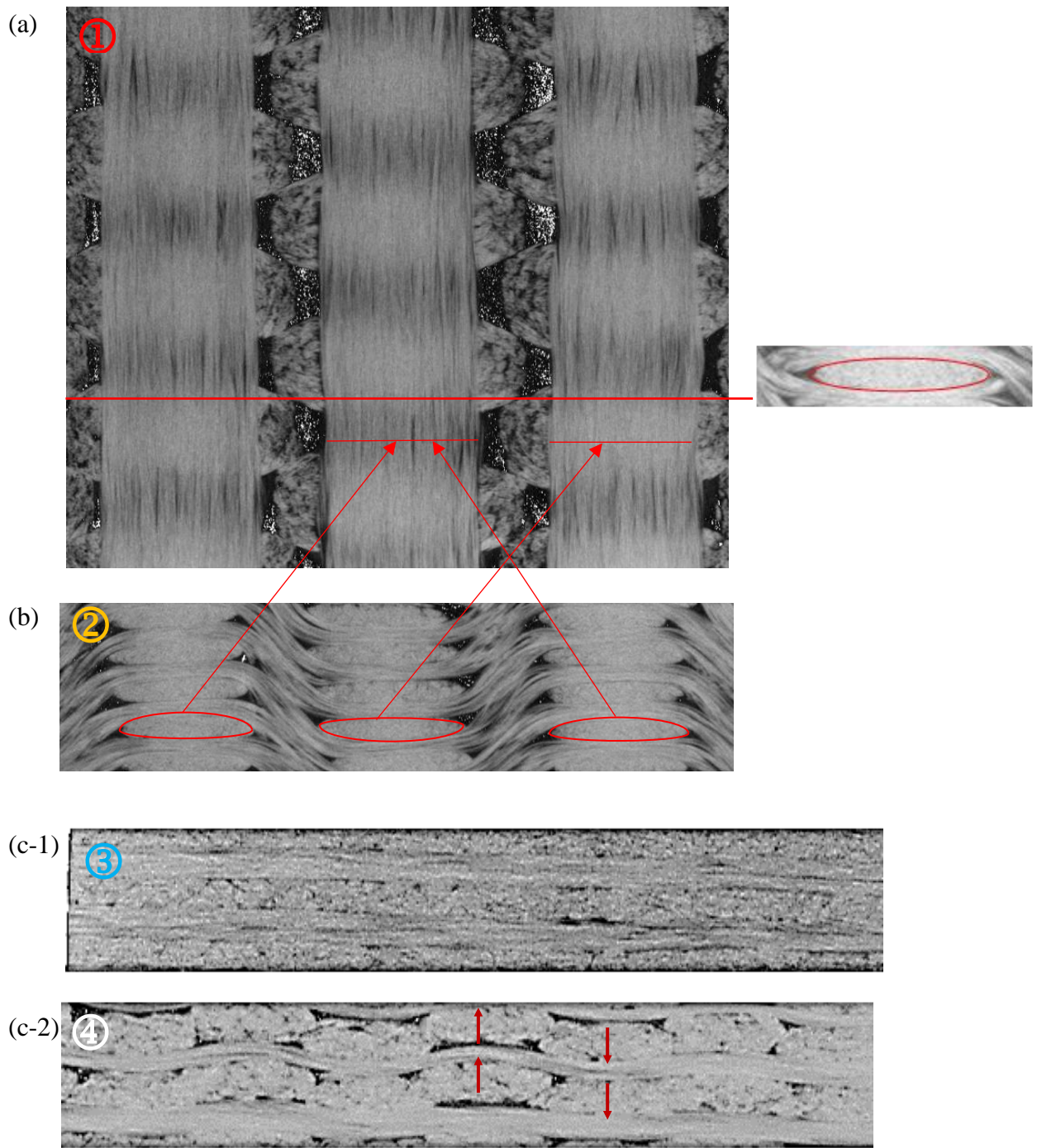


Fig. 3 Micro-CT images of 3D woven composite glass fibre composite: (a) cross-section orthogonal to through thickness direction; (b) cross-section orthogonal to the weft direction; (c) cross-sections orthogonal to the warp direction

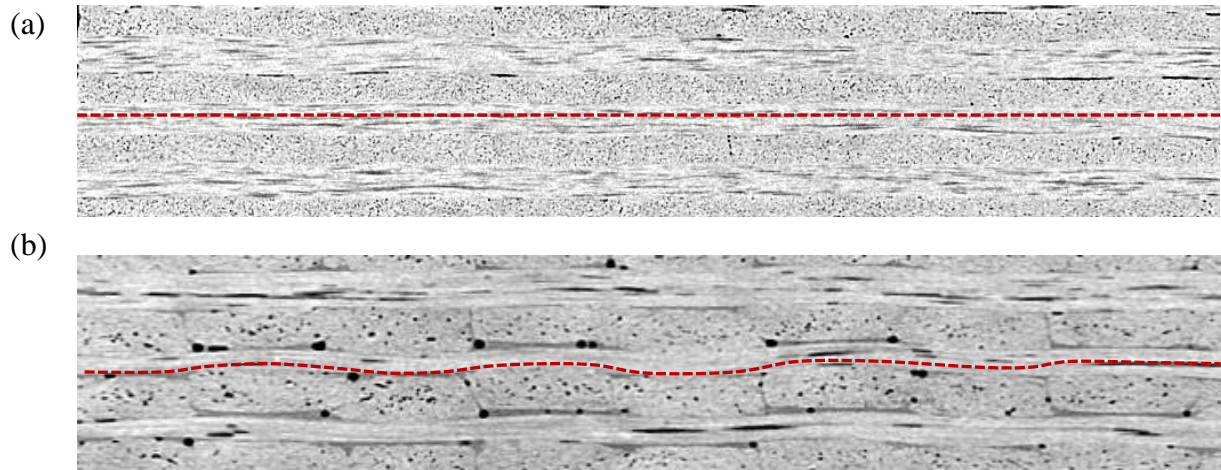


Fig. 4 Micro-CT images of cross-section view of carbon fibre composite orthogonal to warp direction: (a) cross-section is taken through the centre of the weft tow; (b) cross-section taken at the side of the weft tow

3 Parametrisation and implementation of varying weft tow geometry

3.1 Geometric implementation of the cross-section variation along the weft tow path

To reveal the effects of varying weft tow geometry on predictions of the effective properties of woven composites, two models of the weft tow undulations have been proposed as illustrated in Fig. 5. Effectively, in the weave, the originally straight weft tows, as shown in Fig. 5(a), are replaced with the undulating ones. Undulation model shown in Fig. 5(b) implies that the tows remain straight along their paths while the undulations are restricted locally to the sides of the tows. Weft tow geometry in Fig. 5(c) corresponds to a model where a weft tow exhibits overall undulations along its path, in addition to the variations in the weft tow cross-sections as in the previous model. Such undulations are more likely to be observed in the weaves based on fibre tows of relatively low stiffness, such as glass fibres.

These undulations can be reflected in a unit cell that represents the material. According to the parametrisation scheme [11], the unit cell contains a single warp tow along its width. The weft tows in a UC are represented by segments as marked in Fig. 5(c). For the idealised UC with straight tow shown in Fig. 5(a), the shape of such fragment is a cylinder the base of which is the cross-section of the weft tow orthogonal to its centre line. For weft tows with undulations, the cross-sections on the boundaries of the fragments are the same as those in the UC with straight weft tows, while the overall weft tow shape is much more complex. The weft tow fragment in Fig. 6(a) represents a case with local undulations along the sides of the tow, which corresponds to the weft tow geometry variation scenario in Fig. 3 and Fig. 4. To reproduce this

in a model, the curved weft tow path ABC was defined using the TexGen [30] weave modelling software, via interpolating the master nodes and assigning the varying shapes of the weft tow cross-section profiles along this path. To reproduce an overall undulation of the weft tow, as shown in Fig. 6 (b), the weft tow path was kept straight between different cross-sections. By utilising the cross-section profiles and the lofting paths, these undulations in the weft tows are reproduced automatically.

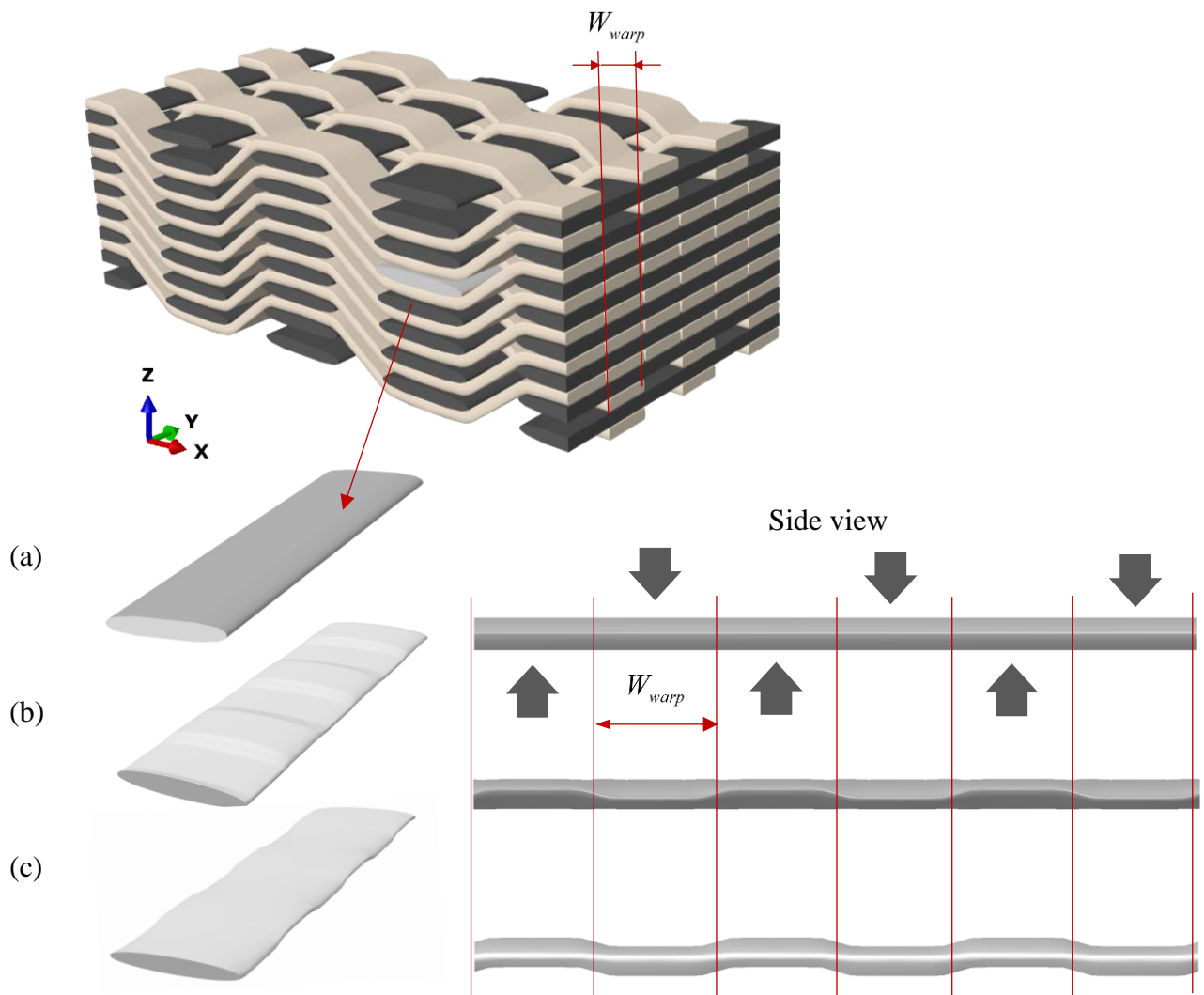


Fig. 5 Models of weft tows undulations: (a) no undulations; (b) local undulations and (c) overall undulations with the weft tow divided into segments of a half-period long each. Directions of the warp tow undulations are shown by grey arrows.

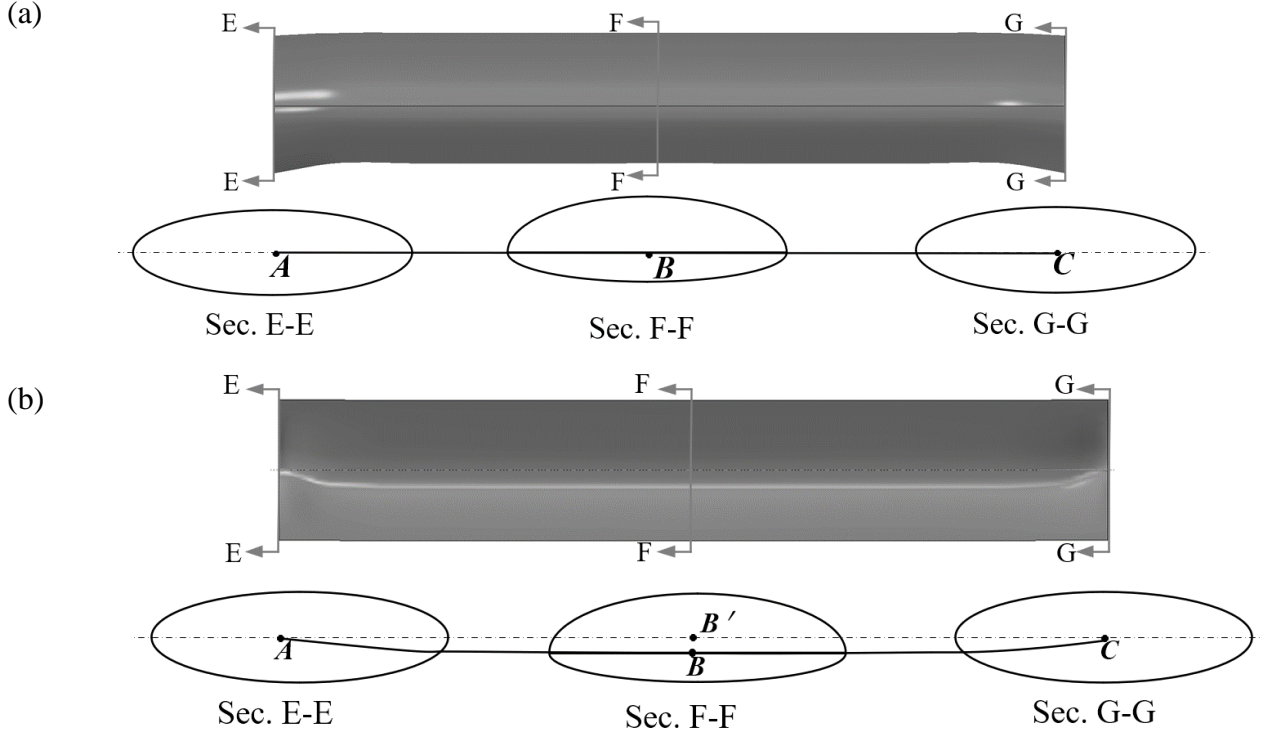


Fig. 6 A segment of the undulating weft tow created by lofting different cross-sections as shown with the lofting paths: (a) straight lofting path ABC corresponding to scenario (b) in Fig. 5; (b) curved lofting path ABC corresponding to scenario (c) in Fig. 5

3.2 Parametrisation of variation in weft tow cross-section

Similar to variations in the weft tow path, the varying cross-section shape of the weft tow has been defined making use of the available functionality in TexGen, which is a lot more versatile than its counterpart in Abaqus. Its shape was idealised as a power ellipse [9]:

$$\begin{aligned}
 x &= \frac{w}{2} \cos(2\pi t) & 0 \leq t \leq 1 \\
 y &= \begin{cases} \frac{h}{2} (\sin(2\pi t))^n & \text{if } 0 \leq t \leq 0.5 \\ -\frac{h}{2} \sin(2\pi t)^n & \text{if } 0.5 \leq t \leq 1 \end{cases} & (1)
 \end{aligned}$$

where w is the yarn width, h is the yarn height, and t is the angular coordinate at the ellipse centre relative to the major axis. Exponent n was introduced as the measure of roundness, varying in the range $[0, 1]$, where zero corresponds to a rectangular, and unity to an elliptical cross-section [30]. Note that the tow cross-section profile can be approximated by substantially more complex geometric shapes [31, 32], if desired. However, this would have made definition of the varying tow cross-section a lot more challenging.

To reproduce the cross-section variation, cross-section profile was further modified as shown in Fig. 7(a). Specifically, it comprises two half-ellipses of different heights, one on top

and another at the bottom. To quantify the extent of variation of the cross-section shape, the variation coefficient of weft tow has been defined as:

$$c = 1 - 2h_2 / (h_1 + h_2) \quad (2)$$

where h_1 and h_2 are double the heights of the upper half ellipse and lower half ellipse. The coefficient c can vary in the range $[0, 1]$, where $c = 0$ corresponds to case where $h_1 = h_2$, while $c \neq 0$ signifies that the cross-section has flattened on one side, e.g. $c > 0$ gives flattened bottom, as shown in Fig. 7(b), and the higher the value of c , the more biased is the appearance of the cross-section.

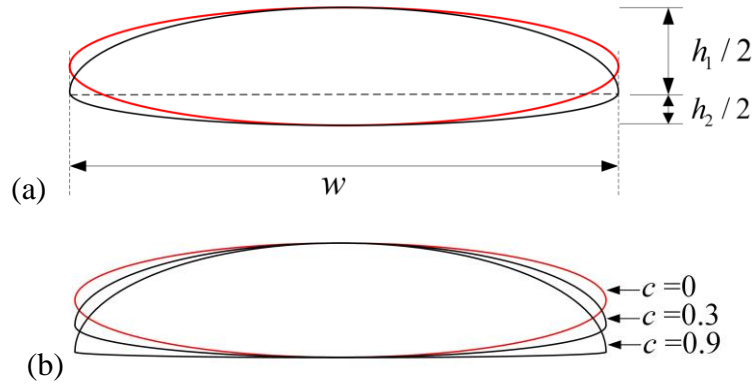


Fig. 7 Varying weft tow cross-section: (a) geometry of the cross-section; (b) change in cross-section profiles associated with different values of coefficient c

The geometric parameters that should be specified to define the varying weft tow cross-section are summarised in Table 1, where restrictions on their selections are also specified. The restriction was to ensure that the weft tow cross-sectional area does not change when the weft tow cross-section geometry is altered. A constant cross-section area is the main assumption used in this parametrisation. Any variation of cross-section area would result in variation of the intra-tow fibre volume fraction and hence the material properties of the tows, definition of which would be challenging. However, for woven composites of layer-to-layer angle interlock type, such as those considered in the present paper, there is no significant change in the weft tow cross-sectional area, as can be seen in Fig. 3, which effectively illustrates a typical weft tow cross-section variation in this type of composites. Therefore, the assumption of the constancy of the weft tow cross-section can be considered reasonable.

Table 1 The geometric parameters of the varying weft tow cross-sections

Geometry	Boundary	Upper ellipse	Lower ellipse	Restriction
Height	h_0	h_1	h_2	$2h_0 = h_1 + h_2$
Width	w_0	w_1	w_1	$w_0 = w_1$
Exponent	n_0	n_1	n_2	$n_0 = n_1 = n_2$

3.3 Parametrisation of variation in the weft and the warp tow paths

One more essential parameter that is employed in parametrisation of the weft tow is the length, l , along which the weft tow path remains straight, and the geometry of cross-section does not change, as shown in Fig. 8. It is defined as:

$$l = (1 - \gamma_{warp}) L_{weft} \quad (3)$$

where γ_{warp} is the measure of roundness of warp tow [11].

When the geometry of the weft tow cross-section varies along its length, it is crucial to ensure that the warp tow conforms to the new geometry, because otherwise a non-physical interpenetration of the tows in the model may occur. The method to define the warp tow paths in a unit cell with straight weft tows has been elaborated in [11] and adopted for the present application. In short, the centre line of the warp tow should remain parallel to the weft cross-section profile. Interference between the adjacent warp and weft tows is prevented by assuming that the warp tow stays in contact with the weft tow until it straightens as it leaves the weft tow, as shown in the magnified and elaborated view of the *OSTR* segment sketched in Fig. 9. It represents the entire warp tow, that can be reproduced by rotating segment *OSTR* by 180° rotation about point *R*, translation along *z*- and *x*-axis (for weaves in which $n_{steep} < n_{deep}$) and then applying a reflectional symmetry about the *yz*-plane.

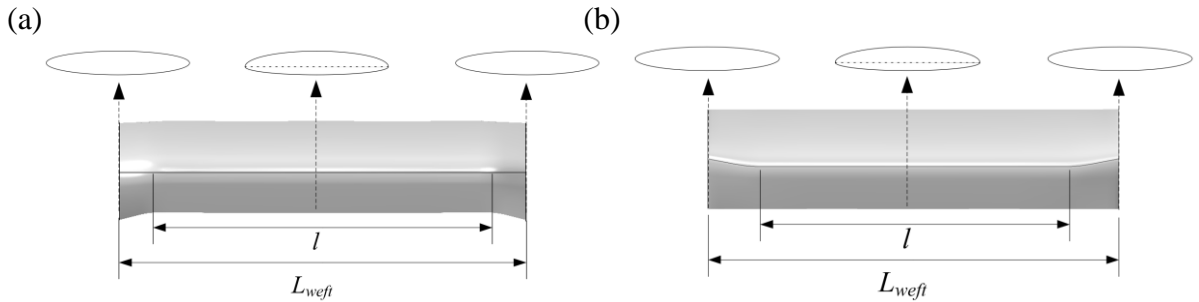


Fig. 8 Cross-section change of the weft tow along its length: (a) tows with localised undulation along the sides; (b) tow with overall undulation

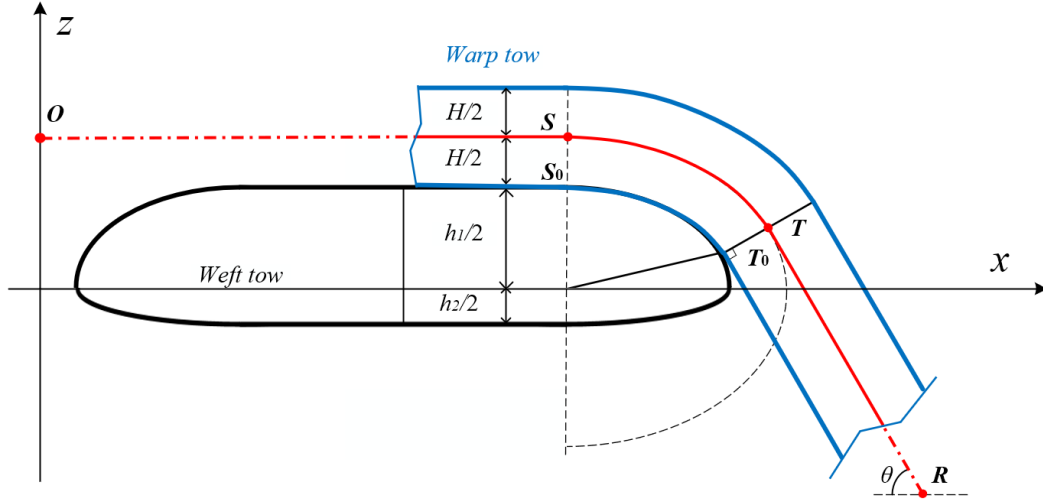


Fig. 9 Geometry of the weft and the warp tow in their contact region

The procedure for defining the sub-segments of $OSTR$ is identical to that established in [11]. The only difference is the need to account for variation in height of the weft tow cross-sections. Because of that, z -coordinate in definition of subsegment OS in [11] should be replaced with

$$z = \frac{1}{2}(H + h_1) \quad (4)$$

The coordinates of the point R should also be replaced by the expressions specified in Table 2, where D_{weft} is the distance between the adjacent weft tow columns.

Table 2 Coordinates of point R

Coordinate	Curved edge as in Fig. 6(a)	Curved centre line as in Fig. 6(b)
x_R	$\frac{1}{2}n_{skip}(w_0 + D_{weft})$	$\frac{1}{2}n_{skip}(w_0 + D_{weft})$
z_R	$-\frac{1}{2}(n_{steep} - 1)\left[H + \frac{1}{2}(h_1 + h_2)\right]$	$-\frac{1}{2}(n_{steep}H + h_1 + h_0)$

3.4 Formulation and implementation of the UC model

The UC modelling has been adopted as the analysis tool for material characterisation. The theoretical background behind the unit cell formulation, including derivations of the relative displacement boundary conditions, load application and effective properties extraction, has been given in full in [13]. The material characterisation procedure, from generating the FE model to post-processing of the results, has been fully automated in Abaqus utilising Python

script, as is also elaborated in [13]. For the 3D woven layer-to-layer angle interlock composite, which is the material under consideration here, the parametrised idealised unit cell model has been established and implemented in [11], where mathematical formulation of the boundary conditions has been given explicitly, and the Python script associated with the characterisation procedure has been verified. In the present work, the script was supplemented with functionality allowing to reproduce the varying cross-section of the weft tow as is defined in the previous subsections. Use of the Python script allows to import the weft tow generated in TexGen to Abaqus, to replace the straight tow weft in the original unit cell model. Once the geometry is modified, the rest of the procedure is followed automatically, namely, the script generates the geometry, prescribes material behaviour to the constituents, defines the relative displacement boundary conditions, and carries out the post-processing of the results. Detailed explanation of how analysis of this kind is conducted is given in [33].

All that is required from the user is to provide the input parameters via the designated user interface. The input comprises the geometric and topological parameters of the woven architecture and the constituent material properties. The geometric and topological input follows parametrisation of the woven composites established in [11]. The topology refers to relative arrangement of the tows within the weave, and for composite considered in the present paper the topological parameters are $n_{offset}=0$, $n_{skip}=n_{step}=1$, $n_{deep}=n_{steep}=2$. This configuration is shown in Fig. 2 and it was selected since it corresponds to a real composite previously analysed and tested in [27]. The definition of topological parameters can be found in [11].

The geometric input parameters have been obtained following recently established procedure [17] which uses the so-called controllable parameters. These are effectively the weaving parameters that have been related to the geometric ones via simple analytical expressions that were derived following the definition of these parameters. The controllable parameters are specified in Table 3, while the geometric parameters obtained from them are given in Table 4. Note that these parameters correspond to the unit cell with straight weft tows. To allow for variation of the weft tow and avoid tow interferences, the measure of the roundness γ_{warp} of the warp tow cross-section is set as 0.2, as opposed to 0.05 that was used in [11], where the latter value was used to reproduce a nearly rectangular warp tow cross-section. Given that the present model involves localised undulations of the weft tow, $\gamma_{warp}=0.2$ was used to ensure that the straight part of the weft tow given by Eq. (3) is not excessively long, as this would deliver excessively steep undulations in the weft tow.

Table 3 Controllable parameters of the woven panels made of IM7 carbon fibre [27]

Fibre	Panel thickness (mm)	Number of warp tows in a column	Number of weft tows in a column	Filament diameter (mm)	Tow count		Tow density (1/cm)	
					warp	weft	warp	weft
IM7	4.2	7	8	5×10^{-3}	12K	24K	10	2.8

The second group of the input parameters were the material properties of the constituents, IM7 carbon fibre tows and Gurit Prime 20LV matrix, and they are also specified in Table 4. The material properties of the tows were determined employing micro-scale characterisation, where the fibre tows were considered as a unidirectional composite. A hexagonal unit cell in a UnitCells© toolbox [33] was utilised to carry out this characterisation in an automated manner.

Table 4 Input properties and parameters for the unit cell

Geometry		Material properties of constituents [34]		
Geometric parameter	Warp	Weft	Matrix (PRIME™ 20LV)	Tow (IM7 CF, $V_f = 78.6\%$)
W (mm)	1.25	2.55	$E = 3.5$ GPa	$E_1 = 217.42$ GPa
H (mm)	0.24	0.33	$\nu = 0.35$	$E_2 = E_3 = 12.21$ GPa
Measure of roundness	0.20	0.90		$\nu_{12} = \nu_{13} = 0.29$
D (mm)	0.05	1.45		$\nu_{23} = 0.45$ $G_{12} = G_{13} = 5.29$ GPa $G_{23} = 4.21$ GPa

Once the formulation of the unit cell is completed by defining appropriate staggered translational symmetry boundary conditions [11], the localised undulation of the weft tows is automatically reproduced. The extent of undulation in Fig. 6 can be varied by assigning different heights to cross-sections at the boundary and in the centre. Two types of undulating weft tows and their corresponding unit cells are shown in Fig. 10. For the case shown in Fig. 10(a), the undulations are restricted to the sides of the weft tow, and the tow generally remains straight when viewed from the side. This represents undulations observed in real textile composites as shown in Fig. 4. The second type of variation, shown in Fig. 10(b), involves substantial overall undulations of the weft tow.

Comprehensive validation of the unit cell-based material characterisation for 3D woven composites has been previously conducted in [17], where the weft tows have been modelled as perfectly straight. Six composites of the same layer-to-layer angle interlock topology but different geometry and/or constituents have been characterised. This included IM7 CF composite as is used in the present study. The elastic characterisation results have been

compared with the respective experimental data, presenting in a systematic way the predictive capability of the method.

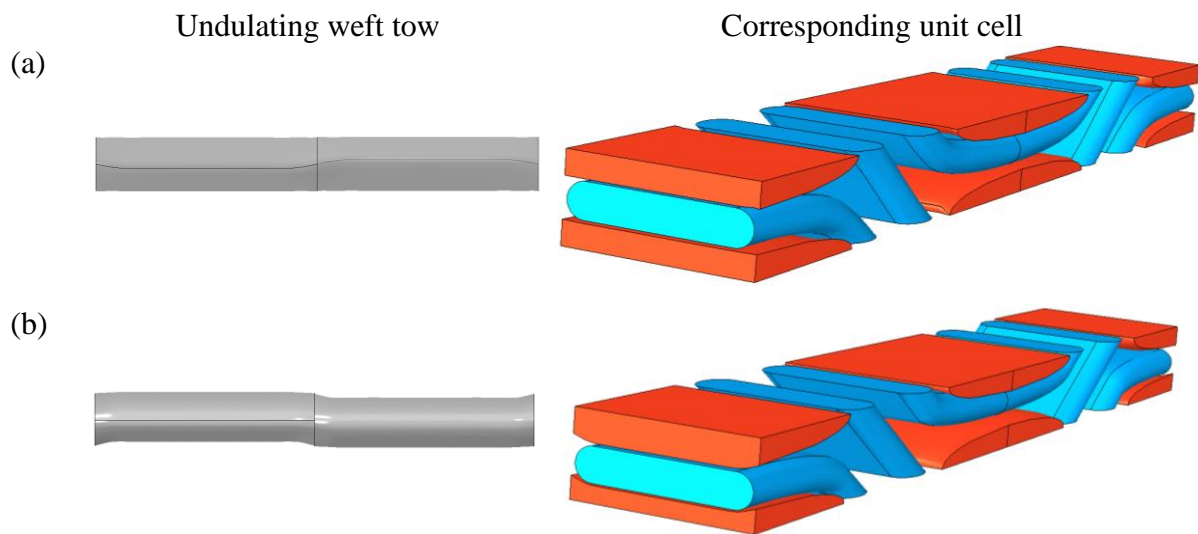


Fig. 10 Two types of undulating weft tows and their corresponding unit cells: (a) undulations are restricted to the edge of the weft tow; (b) overall undulations of the weft tows.

4 Definition of the varying material orientation

While the UC model accounting for the varying weft tow cross-section have been fully formulated in the previous section, there is yet one more aspect of material definition that must be addressed. Specifically, since a tow in a weave comprises a bundle of fibres, any variation in tow cross-section along its path naturally results in variation in the fibre orientation within the tow. In an idealised unit cell, where the weft tows are perfectly straight, the definition of the fibre orientation is straightforward, namely, the fibre direction coincides with that of the tow path. However, when applying the same material orientation to weft tows of varying cross-sections, the fibres on the curved surface become discontinuous. This does not represent the structure of the tow in the real weave. An alternative method is established in this section to allow for the correct definition of varying orientation.

4.1 Available methods for modelling varying intra-tow fibre orientation

It is worth noting that Abaqus [35, 36] offers a functionality for defining the varying material orientation. The user has to specify the material orientation at reference edges, based on which the orientation in the material is reconstructed using a built-in software algorithm. The functionality has been tested on simple 2D shapes shown Fig. 11 and Fig. 12. The

examination of material orientation in Fig. 11 (a) and (b) revealed that the local orientation within the region is uniform and logical when the reference edges were parallel to each other. However, when the reference edges were not parallel, as in Fig. 12(a) and (b), the issue in orientation definition becomes apparent. Specifically, the orientation appears to be defined in a somewhat piecewise linear manner, where up to centre line between the two reference edges orientation is identical to that of the closest reference edge, which results in orientation being discontinuous. If third reference edge is involved, as in Fig. 12(b), same piecewise orientation definition will still be maintained, but it will be between the two adjacent reference edges. Lack of definition of gradual variation of the orientation in Abaqus functionality is apparent.

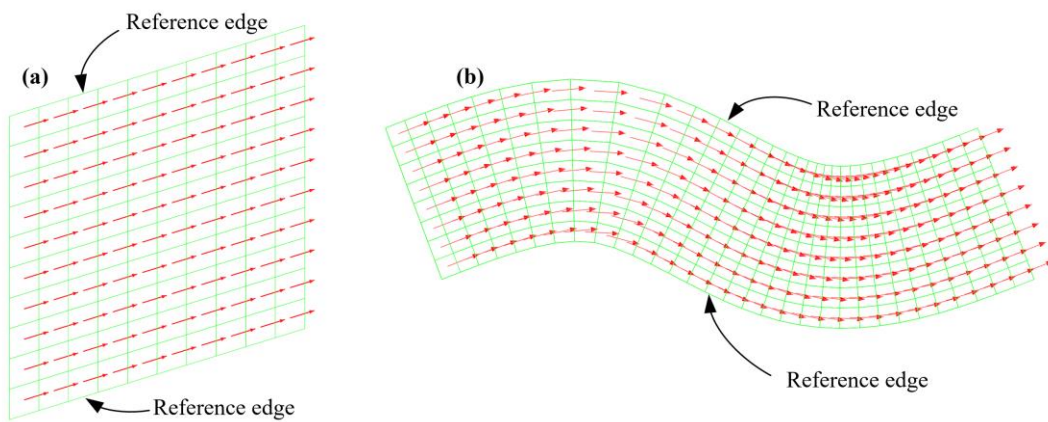


Fig. 11 Abaqus built-in orientation function prescribed between two parallel reference edges: (a) straight edges; (b) curved edges

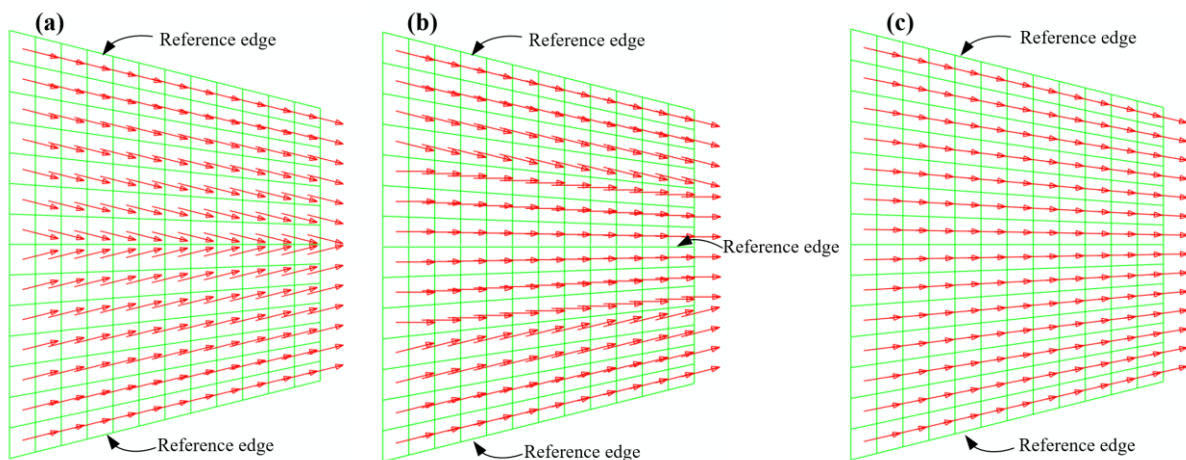


Fig. 12 Material orientation in shapes where reference edges are not parallel: Abaqus built-in orientation based on (a) two reference edges; (b) three reference edges, and (c) orientation defined following procedure established in subsection 4.2

There is also a functionality for defining smoothly varying fibre orientation in weave modelling software TexGen [30]. However, the procedure used for this purpose involves a computationally demanding iterative process, where the intra-tow fibre orientation is calculated by making use of the mesh generated in a certain way. In the present study, more efficient methodology to achieve the same is established and will be presented in the next subsection.

4.2 Theoretical formulation for varying intra-tow fibre orientation

To model the material orientation that would vary smoothly and conform to the shape of the weft tow, linear interpolation between orientation along the straight centre line as a reference and that of a corresponding point on the surface of the tow has been employed. Consider a curved tow as is illustrated in Fig. 13. For any integration point A inside the tow, a section can be introduced as shown in Fig. 13, which passes point A and is perpendicular to the y -axis. The section intersects the centre line of the tow at point O which shares the common y -coordinate with point A and hence can be easily determined as $O(x_O, y_A, z_O)$. For the ease of manipulations, the coordinates of point A can be expressed in a cylindrical coordinate system as $A(y_A, \theta_A, r_A)$ about an axis parallel to the y -axis of the original cartesian coordinate system passing point O , where $r_A = \sqrt{(x_A - x_O)^2 + (z_A - z_O)^2}$ and $\theta_A = \arccos((x_A - x_O)/r_A)$. The direction of this axis is shown as \vec{p}_0 in Fig. 13. The original cartesian coordinates of $A(x_A, y_A, z_A)$ can be obtained from Abaqus as those at an integration point.

Along the radial direction OA , a point can be found on the surface of the tow. The element in the tow containing that point can be identified from inside Abaqus. Take the integration point of the element nearest to that point as an approximation and label it as point B . The coordinates of point B are readily available from Abaqus. Converting them to the same cylindrical coordinate system, one obtains $B(y_A, \theta_A, r_B)$, where $r_B = \sqrt{(x_B - x_O)^2 + (z_B - z_O)^2}$. Then the principal vector \vec{p} , indicating the fibre orientation at point B , can be calculated as:

$$\vec{p} = \vec{n} \times \vec{s}, \quad (5)$$

where \vec{n} is the normal to the surface of the element in which point B is located as is available directly from Abaqus and unit vector $\vec{s} = \vec{n} \times \vec{p}_0 / |\vec{n} \times \vec{p}_0|$ with \vec{p}_0 given as the direction of the axis of the cylindrical coordinate system, which is defined, in the current coordinate system, as:

$$\vec{p}_0 = [0 \ 1 \ 0]^T. \quad (6)$$

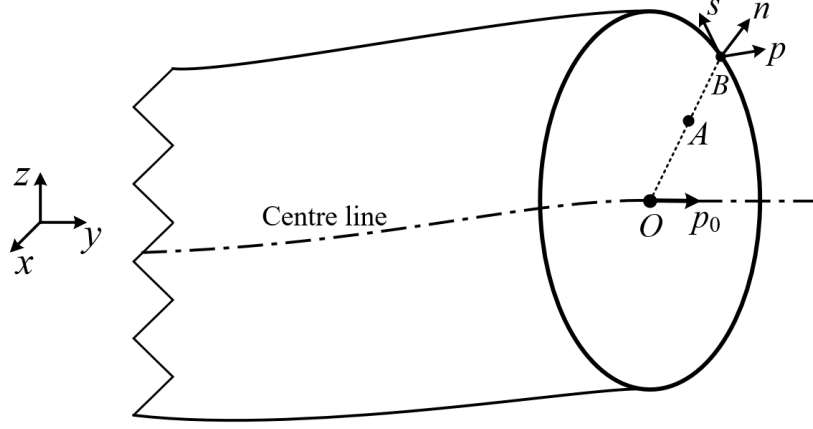


Fig. 13 Determination of principal vector \vec{P} at point B , perpendicular to \vec{n} and \vec{s} respectively

For any integration point A inside the tow domain, the unit vector \vec{p}_A can be thus linearly interpolated between the \vec{p}_0 and \vec{p} as:

$$\vec{p}_A = \frac{(1-\rho)\vec{p}_0 + \rho\vec{p}}{|(1-\rho)\vec{p}_0 + \rho\vec{p}|}. \quad (7)$$

where the factor ρ is the ratio of the radial distance between point A inside the tow domain and its corresponding point B approximately on the surface along the radial line OA :

$$\rho = \frac{r_A}{r_B}. \quad (8)$$

Principal vector \vec{p}_A is used to define the material orientation at any point A inside the tow. As an illustration, the procedure has been applied to define the material orientation within the trapezoidal part in Fig. 12(c). The gradual smooth variation of the orientation is apparent, as opposed to discontinuous appearance in Fig. 12(a) and (b).

It should be noted that the linear interpolation between the orientation on the surface and that along the centreline has also been adopted in [37]. However, the orientation on the surface there was determined as local tangent to discrete lines near the surface of the fibre tow that represented the fibre bundles. The procedure established in the present paper is therefore more universally applicable since it does not require such sophisticated definition of the tows.

4.3 Implementation of the varying material orientation in FE models

In the finite element model of the tow, the principal vector has been interpolated at each element between the exterior surface and centre tow path. This has been carried out automatically, making use of the Python script written specifically for this purpose. The obtained orientation has been prescribed to the weft tows within the UC as a discrete field, which is a functionality available in Abaqus.

Table 5 Geometric parameters of the altered weft tow

	Non-biased ellipse	Upper ellipse	Bottom ellipse
Width (mm)	2.55	2.55	2.55
Height (mm)	0.33	0.23	0.43
Exponent n	0.9	0.9	0.9

To visualise the material orientations obtained using different fibre orientation models, the undulating weft tow shown in Fig. 8(b) has been used as an example. The variation coefficient (1) in this example has been set to 0.3 to exaggerate the curviness of the weft tow, which facilitates the demonstration of the fibre orientations. The geometric parameters of the weft tow cross-section corresponding to such coefficient of variation are given in Table 5.

The fibre orientations assigned using three different methods are shown in Fig. 14, where the red arrows/lines indicate the local directions of fibres. The fibre paths in each case are also sketched in the insets of the respective images. The first method was to assign the identical orientation at all elements within the tow. As can be seen in visualisations of the orientation over the weft tow in Fig. 14(a), the orientation does not change from element to element and, because of this, becomes discontinuous on the tow surface in the curved region. This discontinuity is highlighted in red in a schematic inset to Fig. 14(a). Essentially, this mimics broken fibres in the tow, which is obviously unacceptable. This error is easy to detect.

The second method was to employ built-in algorithm in Abaqus utilising the reference edges and faces. As shown in Fig. 14(b), it produces piecewise linear definition of orientation that has been already discussed in subsection 4.1. The discontinuity in orientation in this case is highlighted in red in a schematic inset to Fig. 14(b). Same as in the previous case, it is wrong, but is now harder to detect because the discontinuity has been hidden inside fibre tows. Finally, orientation in Fig. 14 (c) was produced following the procedure established in the present paper. As can be seen, the continuous straightening of the fibre orientation from the external surface towards the central axis of the tow was achieved and the fibre orientation follows the

variation of the geometry in general. The orientation therefore conforms to the complex shape of the tow. Same conforming orientation has been reproduced using this newly established orientation definition method in a simple 2D shape in Fig. 14(c).

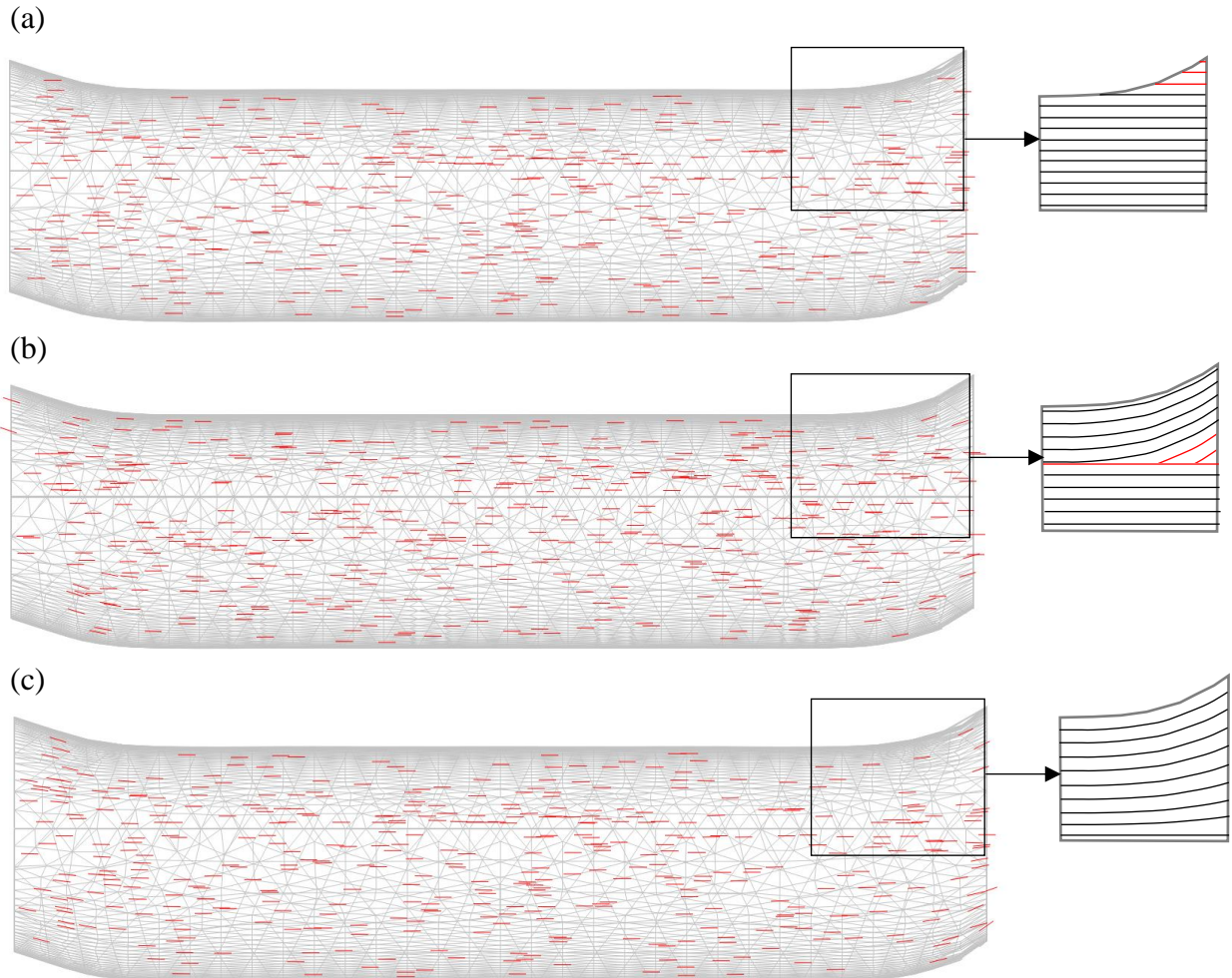


Fig. 14 Fibre orientations in a curved weft tow: (a) constant orientation; (b) varying orientation as provided in Abaqus [36]; (c) conforming orientation

5 Effect of weft tow variation on material characterisation results

To assess how significantly the varying weft cross-sections can affect the predictions of the effective elastic properties of the textile composites, the two undulation models have been applied separately as two case studies. The modelling tools utilised and the material systems used in both exercises were detailed in subsection 3.4.

In the first case study, the variation of the weft tow represented that in real textile composite shown in Fig. 4. The weft tow geometry for such case is shown in Fig. 15(a), where

undulations are restricted to the sides of the weft tow, and the tow generally remains straight when viewed from the side. In the second case study, the weft tow had substantial overall undulations, as shown in Fig. 15(b). A range of material characterisation cases have been carried out, where the variation coefficient in Eq. (1) has been assigned values in the range from 0 to 0.3. The maximum value of the coefficient of variation was chosen such that it would deliver undulation that would apparently be exaggerated compared to the one in a real composite in Fig. 4(b). The latter has not been quantified through measurements, because the objective of the present paper is to expose the sensitivity, if any, of the elastic properties to undulations in the weft tows, rather than consider any isolated case. The variations in heights of the upper and lower half ellipses are specified in Table 6. They are obtained for each value of the variation coefficient using Eq. (2) and the restriction specified in Table 1. The larger the value of the coefficient, the higher is the extent of undulations in the weft tows, either localised or the overall ones, as is illustrated in Fig. 15(a) and (b), respectively. The width and measure of the roundness of the cross-sections are given in Table 5.

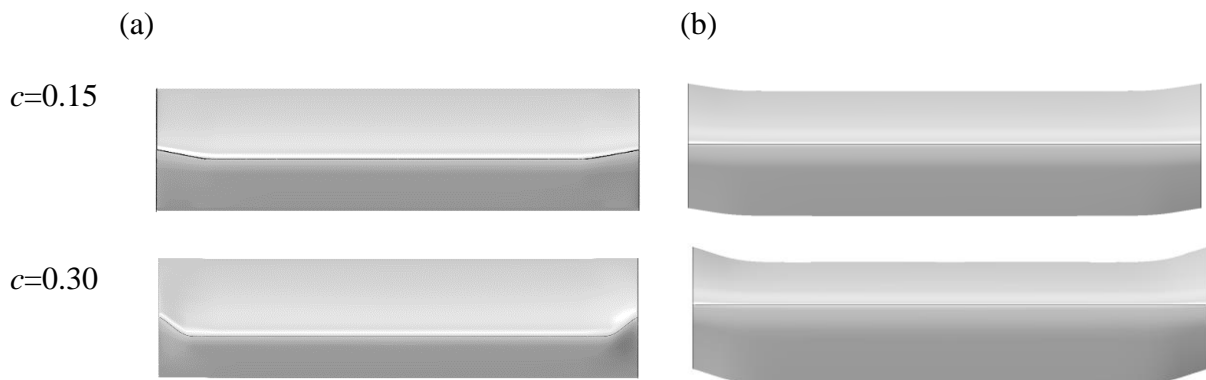


Fig. 15 Variation in weft tows shape associated with different values of the variation coefficient: (a) tow with undulations along the sides; (b) tow with curved centre line

Table 6 Geometric parameters of the varying cross-section of weft tow

Variation coefficient c	0	0.05	0.10	0.15	0.20	0.25	0.30
h_1 (mm)	0.33	0.34	0.36	0.38	0.39	0.41	0.43
h_2 (mm)	0.33	0.32	0.30	0.28	0.27	0.25	0.23

5.1 Case study 1: Localised undulations

As initial assessment of the changes in the UC models associated with varying tow geometry, the geometric properties has been considered as listed in Table 7. The volumes of the tows and of the UC were obtained as the by-product of the numerical analysis, by requesting their output from Abaqus, where they are calculated using readily available functionality. The interlocking angle is calculated based on the geometric parameters given in Table 4 using the procedure established in [11]. The volume of the weft tow was expected to be constant because the area of the cross-sections was kept constant along the weft path while its geometry was varying. However, there was slight deviation in its value between the different cases. This was due to the use of the lofting function. Specifically, while the areas at the profiles are meant to be constant, there is a slight deviation between the adjacent profiles. This deviation can further be reduced by reducing the distance between the adjacent profiles. On the other hand, slight variation in the warp tow geometry was genuine, and it was associated with the changes in geometry of the adjacent weft tow and hence the subtle variation of the warp tow path. Change in the warp tow path is also responsible for the reduction of the interlocking angle from 31.53° at $c=0$ to 29.36° at $c=0.3$.

The calculated effective elastic properties are also summarised in Table 7. The change of the properties obtained with the configurations having weft tow undulations relative to configuration with straight weft tows ($c=0.0$) is plotted in Fig. 16. It was found that the most affected effective stiffness property was the weft Young's modulus, which decreased by 2.2% as the variation coefficient reached 0.3. This trend is reasonable, because presence of undulations in the tows aligned in certain direction results in reduction of elastic moduli associated with that direction. It is worth noting that the effective weft moduli predicted using the UC model with straight weft tows for six different woven composites in [17] were found to consistently (five cases out to six) exceed their experimental counterparts. Specifically, for composite based on IM7 tows as is considered in the present paper, the experimental value of the effective weft modulus was 62.7GPa. The results therefore show that the lack of representation of the localised undulations in the idealised UC model is indeed responsible for some overprediction of the weft effective elastic modulus. While the 2.2% reduction in the weft modulus in the present case does not seem like a significant change, the effects of localised undulations can potentially be more pronounced for other constituents and composite geometries. A comprehensive study of this kind would require a substantial effort and is beyond the scope of the present paper whose main objective is to establish the capability for

incorporating this varying feature, while IM7 carbon fibre composite has been chosen to demonstrate the functionality of the method proposed.

Table 7 Geometric and effective elastic properties over a range of variation coefficients for model with localised weft tow undulations

Geometric properties							
Coefficient of variation	0.0	0.05	0.10	0.15	0.20	0.25	0.30
Interlocking angle, °	31.53	31.15	30.78	30.41	30.05	29.70	29.36
Volume of unit cell, mm ³	5.928	5.928	5.928	5.928	5.928	5.928	5.928
Volume of weft tow, mm ³	1.632	1.632	1.631	1.631	1.631	1.632	1.631
Volume of warp tow, mm ³	2.410	2.410	2.410	2.410	2.411	2.411	2.412
Effective properties							
E_x (GPa)	43.84	43.90	43.94	43.97	43.97	43.97	43.95
E_y (GPa)	65.90	65.78	65.65	65.42	65.15	64.87	64.48
E_z (GPa)	9.22	9.22	9.23	9.23	9.23	9.24	9.24
G_{xz} (GPa)	2.91	2.90	2.90	2.90	2.90	2.90	2.90
G_{yz} (GPa)	4.81	4.81	4.80	4.80	4.80	4.80	4.79
G_{xy} (GPa)	3.40	3.39	3.39	3.39	3.40	3.39	3.39
ν_{xy}	0.0023	0.0068	0.0116	0.0162	0.0205	0.0246	0.0280
ν_{xz}	0.8785	0.8788	0.8784	0.8778	0.8770	0.8763	0.8757
ν_{yz}	0.4272	0.4250	0.4230	0.4214	0.4204	0.4200	0.4203

Minor increase in the warp effective elastic modulus is associated with the marginal straightening of the warp tows, which is reflected in the reduced value of the interlocking angle. The property found to be the most sensitive to cross-section geometry variation was the Poisson's ratio ν_{xy} , increasing from 0.0023 to 0.028 as the variation coefficient increased from 0 to 0.3. Simultaneously, Young's modulus in the weft direction reduces marginally with the variation coefficient. Both trends are reasonable, because the weft tows with undulations are more compliant than their straight counterparts hence it is natural to expect that reducing weft Young modulus (in y-direction) is accompanied with increasing Poisson's ratio ν_{xy} . Often, researchers and practitioners do not give enough attention to Poisson's ratios, which sometimes can underline important mechanical intricacies, such as the success of the adoption of the so-called quasi-isotropic laminates at the early stage of the development of structural applications of composites, the most undesirable but also unavoidable free edge effect, anticlastic deformation, etc.

The variation of the remaining effective properties was marginal, within 1%.

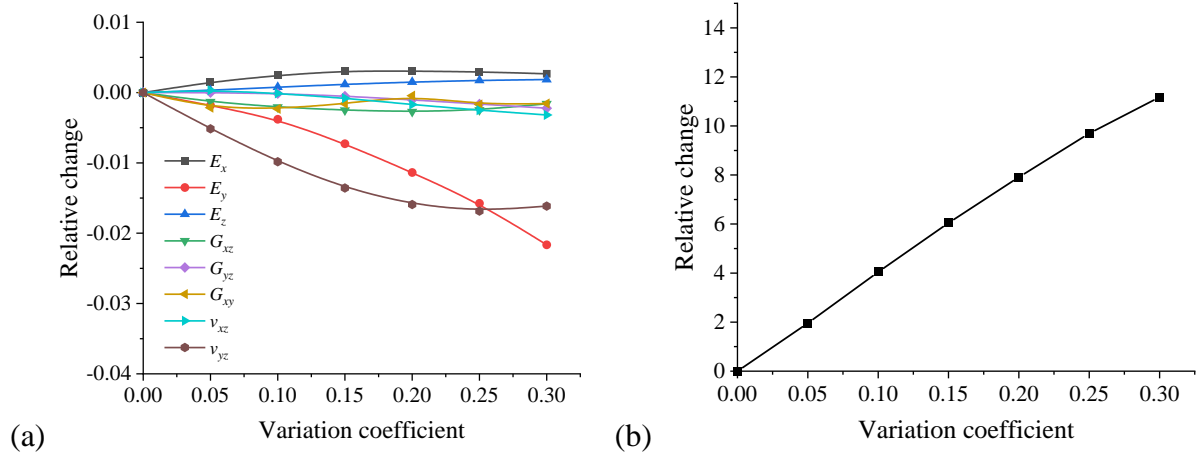


Fig. 16 The relative change of effective elastic properties predicted with models having localised undulations of the weft tows: (a) properties for which the absolute relative change was below 0.03; (b) Poisson's ratio ν_{xy}

The low value of Poisson's ratio ν_{xy} , which is a lot smaller than the typical values for the UD composites [38], is a characteristic of 3D woven composites of layer-to-layer angle interlock architecture. The causes for this have been explained in [11]. In short, when the composite is stretched along the direction of weft tows, the inclined parts of the warp tows rotate, becoming less inclined, as a result of the deformation. Thus, there is an expanding trend in the warp direction, competing with the natural tendency of contraction due to the Poisson's effect. The rotations of the parts of the warp tows also result in the contraction in the thickness direction in addition to the natural Poisson's effect in the same direction. This is manifested by large value of ν_{xz} as is also shown in Table 7.

5.2 Case study 2: Overall undulations

Similar case study was carried out for the configuration where the weft tows were undulating along their paths, as shown in Fig. 15(b). Same as in the previous case, the higher are the values of the variation coefficient, the more pronounced are the undulations of the weft tow. The values of heights of half ellipses, h_1 and h_2 , that are essential for definition of such undulation, will be the same as in Table 6 but reversed in this case, because, referring to Fig. 15(b), it is the height of the half ellipse forming top of the cross-section that should be reduced.

In general, the effective elastic properties obtained in this case study and summarised in Table 8, and their relative changes plotted in Fig. 17 reproduce the same qualitative trends as were revealed in the previous case study. Quantitatively, the change in the elastic properties was more substantial in this case, namely, the elastic modulus E_y along the weft direction reduced by $\sim 12\%$ at $c=0.3$ as opposed to $<3\%$ in the previous case study. The warp modulus

increased by 3% as opposed to <1% in the previous study. A novel feature was noticeable reduction, by 6%, in effective shear elastic modulus G_{yz} , and Poisson's ratio ν_{xz} , which were marginally affected by tow geometry variation in the previous case study. The Poisson's ratio ν_{xy} remained the most affected property, but the relative change in its value at maximum variation coefficient nearly doubled compared to that in the previous case study.

Table 8 Geometric and effective elastic properties over a range of variation coefficients for model with overall weft tow undulations

Geometric properties	0	0.05	0.10	0.15	0.20	0.25	0.30
Interlocking angle, °	31.53	31.42	31.31	31.21	31.11	31.02	30.93
Volume of unit cell, mm ³	5.928	5.928	5.928	5.928	5.928	5.928	5.928
Volume of weft tow, mm ³	1.632	1.632	1.632	1.632	1.632	1.632	1.632
Volume of warp tow, mm ³	2.410	2.329	2.327	2.324	2.322	2.320	2.318
Effective properties							
E_x (GPa)	43.84	44.01	44.18	44.33	44.47	44.59	44.69
E_y (GPa)	65.90	65.88	64.79	63.62	61.96	60.20	58.39
E_z (GPa)	9.22	9.23	9.24	9.24	9.24	9.24	9.24
G_{xz} (GPa)	2.91	2.90	2.90	2.91	2.91	2.92	2.93
G_{yz} (GPa)	4.81	4.75	4.70	4.65	4.60	4.55	4.50
G_{xy} (GPa)	3.40	3.39	3.40	3.39	3.40	3.40	3.40
ν_{xy}	0.0023	0.0111	0.0194	0.0271	0.0341	0.0404	0.0458
ν_{xz}	0.8785	0.8679	0.8577	0.8478	0.8382	0.8289	0.8199
ν_{yz}	0.4272	0.424	0.4225	0.4223	0.4239	0.4258	0.4282

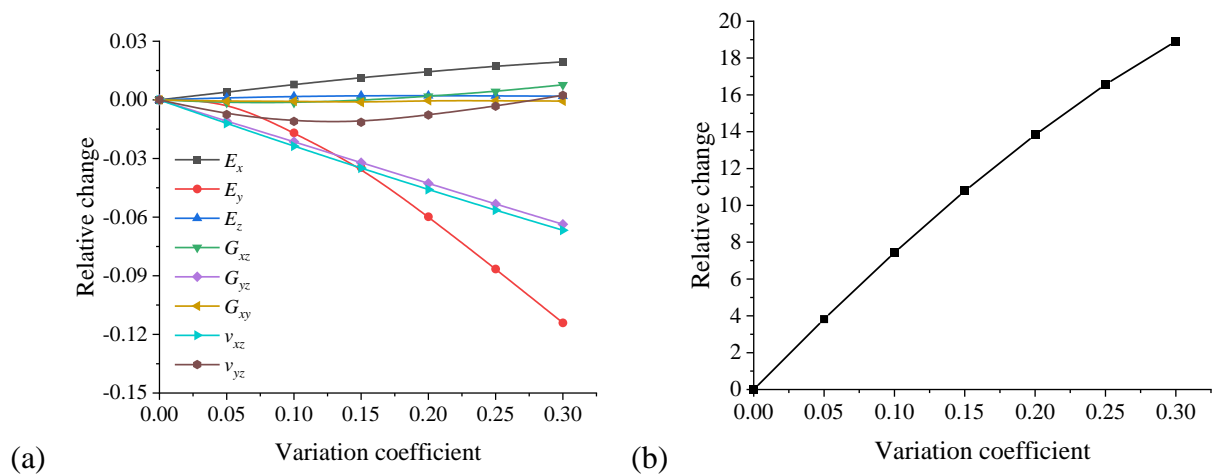


Fig. 17 The relative change of effective elastic properties predicted with models having overall undulations of the weft tows: (a) properties for which the absolute relative change was below 0.15; (b) Poisson's ratio ν_{xy}

Table 9 The effective elastic properties predicted with different fibre orientations

Properties	$c=0$	$c=0.3$		
		Constant orientation	Abaqus orientation	Conforming orientation
E_x (GPa)	43.84	44.65	44.76	44.69
E_y (GPa)	65.90	59.73	56.43	58.39
E_z (GPa)	9.22	9.24	9.22	9.24
G_{xz} (GPa)	2.91	2.90	2.94	2.93
G_{yz} (GPa)	4.81	4.49	4.49	4.50
G_{xy} (GPa)	3.40	3.39	3.39	3.40
ν_{xy}	0.0023	0.0207	0.0204	0.0458
ν_{xz}	0.8785	0.8281	0.8292	0.8199
ν_{yz}	0.4272	0.4260	0.4369	0.4282

This study shows that overall undulation of weft tows affects the effective elastic properties more than the undulations localised to the sides of the weft tows. It would also be informative to assess how the results would change if different orientation definition was used. To do so, two more material characterisation cases was carried out where the material orientations in the weft tow were defined as shown in Fig. 14(a) and (b).

The results are given in Table 9 along with those obtained previously for the unit cell with straight weft tows and one with smoothly varying orientation, which were included for ease of comparison. Compared to the results obtained with the model having straight weft tows, the most significant difference was the values of the weft modulus, E_y , and the Poisson's ratio ν_{xy} . The value of the weft stiffness obtained for model with conforming (correct) orientation was found to be closer to that corresponding to the model with constant orientation. This signifies that at least as far as the modelling of varying geometry of the weft tow is concerned, Abaqus functionality for representing the varying material orientation does not produce any tangible improvement to the accuracy of prediction as compared to the constant orientation.

5.3 Non-physical stress concentrations due to inconsistent definition of material orientation

The analysis reported above suggests that as far as the elastic characterisation of woven composites is concerned, lack of consistency in definition of material orientation has little effect on predictions of the elastic properties.

However, drastic differences can be observed in the obtained stress distributions. To demonstrate them, three simplistic models as shown in Fig. 12 were loaded in tension in x -direction. The contours of the direct stress in global x -direction and the shear stress are shown in Fig. 18. The fictitious stress concentrations are present in σ_{xx} stress contours shown in

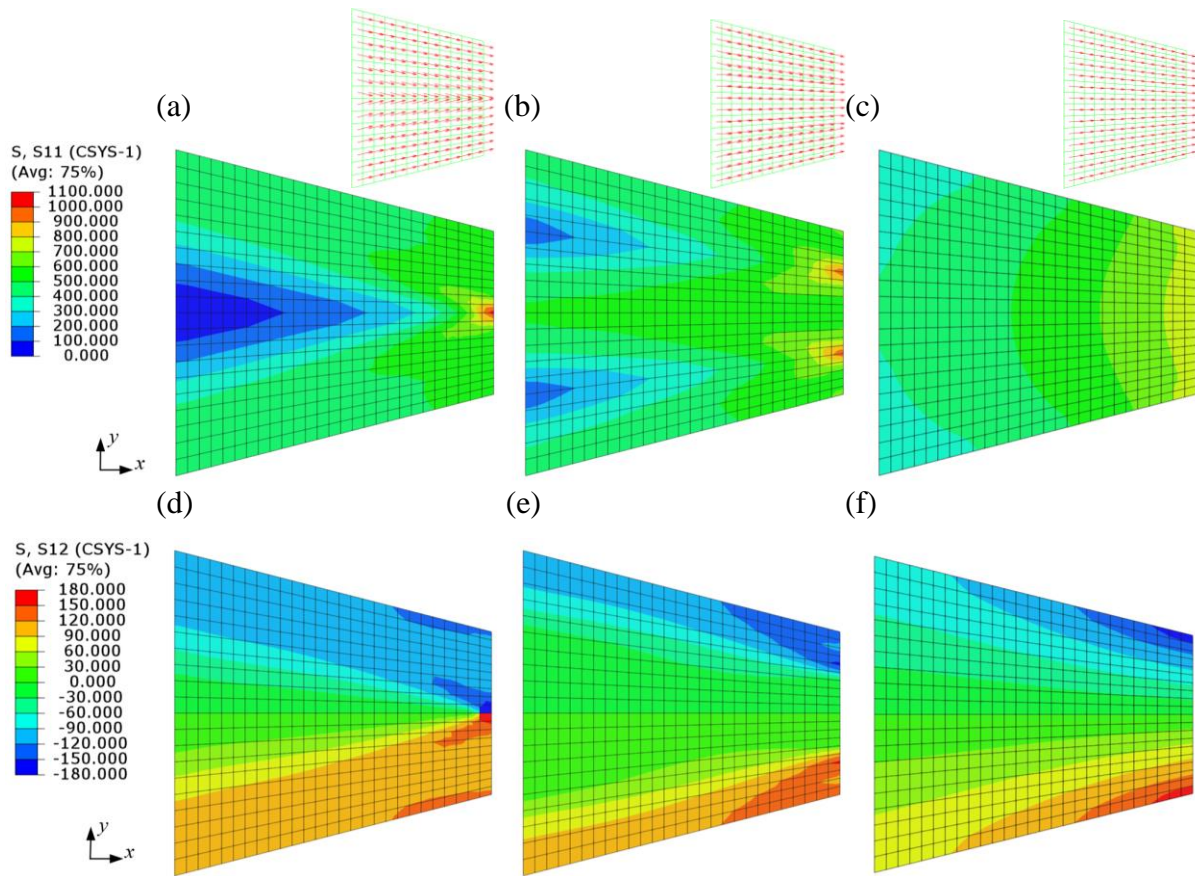


Fig. 18 The stress contours predicted with different fibre orientations: (a), (d) Abaqus material orientation based on two reference edges, (b), (e) Abaqus material orientation based on three reference edges, (c), (f) continuous orientation variation established in Section 4.

Fig. 18(a) and (b) when Abaqus functionality for orientation definition was employed with the two outer inclined edges as references. The location of these stress concentrations coincides with the discontinuity of fibre paths as represented by the orientation employed. Similar stress concentration in the shear stress τ_{xy} field can be observed in Fig. 18(d) for the same reason. When three reference edges are used, i.e. with the centreline as an additional reference, stress concentrations in τ_{xy} distribution vanish superficially, while they are still present in σ_{xx} contour in Fig. 18 (b), again, located at the position of fibre discontinuity, hence two locations. These fictitious stress concentrations can be hidden to a degree if the stresses were plotted in their materials' principal axes (plots not shown but not difficult to envisage), i.e. in terms of σ_{11} and τ_{12} , respectively. A critical observation would reveal that the magnitudes of these stresses show reasonable continuity across the interface where the two different orientations from two individual references meet. However, since material orientations across the interface

are different, stress directions would also differ on two sides of this interface, implying an artificial discontinuity in the material. The stress distributions as shown in Fig. 17(c) and (f), predicted using the conforming material orientation developed in the present paper, are free from such fictitious stress concentrations both in the materials principal axes (not shown) and the global coordinate system, since there is no artificial discontinuity in fibre paths.

Since damage initiation and propagation and the subsequent ultimate failure are closely associated with the stress concentrations present in the material, fictitious stress concentration resulting from poor definition of material orientation will certainly introduce errors in strength prediction. The consistent and convenient methodology for orientation definition as was established in the present paper will help rule out artificial error of this kind.

5.4 Stress state variation associated with the weft tow undulations

With the erroneous definition of fibre orientation being ironed out in the previous subsection, one should have improved confidence on the predicted stresses which are essential for the subsequent strength predictions. Although systematic strength predictions are seen as a future development for a subsequent publication to address, it is insightful to demonstrate the differences the undulations in the weft tows make on the stress distribution. The longitudinal stress contours over the straight and the curved weft tows are compared in Fig. 19. For all these cases, the respective unit cells were loaded in tension along the weft direction, as an example. As can be seen in Fig. 19(a), the stress in the fibre direction was generally uniform in the straight weft tows. In the weft tow with undulations along the sides, the stress concentrations were predicted that were localised to the curved parts of the tow, as shown in Fig. 19(b). In weft tow with overall undulations, higher stress levels are apparent over its curved region, as can be seen in Fig. 19(c). In general, the higher the stress levels, the more critical the stress state to potential failure of the material or the damage initiation and propagation in the material, although systematic explorations of this kind are beyond the scope of the present paper. It is clear that, as an idealisation, straight weft tows are simple to model and they present as a reasonable approximation as far as effective elastic properties are concerned. However, they could lead to misrepresentation of the possible stress concentrations caused by lack of undulations, which are inevitable in physical reality and should be duly represented to strength characterisation exercises. In particular, the idealisations with straight weft tows tend to underestimate the stress level, which would potentially lead to a risky prediction of eventual failure of such a composite and hence would not be a comfortable position in any practical

engineering design. A proper study on the prediction of strength of such composites will be the subject of a future development.

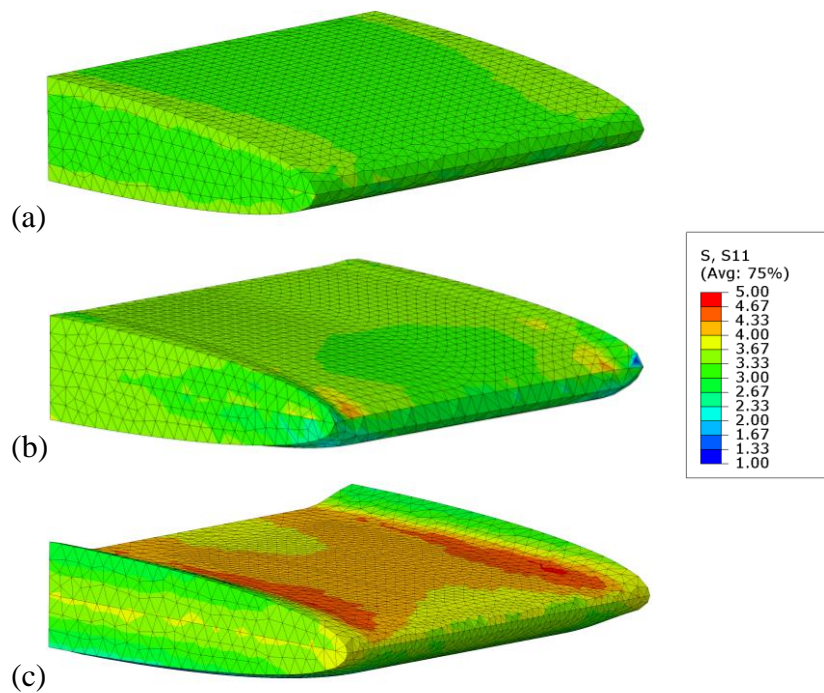


Fig. 19 Stress contours over the weft tow:(a) straight weft tow; (b) weft tow with localised undulations along the sides ($c=0.3$); (c) weft tow with overall undulations ($c=0.3$)

6 Conclusions

The minor undulations of the straight weft tows have been satisfactorily simulated. For this, two parametrised models have been established, addressing different types of undulations. They have been implemented in a unit cell for 3D woven composites, so that the unit cell can be applied in an automated manner.

To assess the effects of such undulations consistently, formulation of the varying material orientation has been established and implemented. The need for this development was caused by inferiority of functionality for defining the varying material orientation that is available in Abaqus. The latter defined the variation of orientation in a piecewise-constant way with the interfaces between these parts of different orientations planted as fictitious material discontinuities. While such overly simplistic definition of orientation was found to have generally negligible effect on the predictions of the effective elastic properties, it will introduce fictitious stress concentration pockets in the overall stress distribution, which would be detrimental in any strength characterisation exercises. It was demonstrated via a simple example that the newly established procedure for orientation produces smooth variation of material orientation and the associated stress contours are free from the unreasonable stress

concentrations. This should pave a way forward towards systematic predictions of strength of 3D woven composites.

The effects of variable weave architecture on predictions of the elastic response of 3D woven layer-to-layer angle interlock composites have been revealed. The numerical analysis has shown that the relative change between the elastic properties obtained with the model having straight weft tows and one having localised undulations along the edges of weft tows was within 3%, and it can exceed 10% for the models with overall undulations. Even so, this is not overwhelmingly significant and hence justifies neglecting this variation when carrying out the elastic characterisation of this type of woven composites. However, whether the variation of the weft tow geometry can safely be neglected or not, depends on the nature of the problem. While its effects on the effective elastic properties are not pronounced, it has been shown that this subtlety could have significant effects on the local stress distribution, implying their knock-on effects on the strength predictions for woven composites. This indicates that in problems involving damage and failure, the minor undulations in the weft tows should not be dismissed without due consideration. This will be addressed in full as a subsequent development.

Declaration of conflicting interests

The Authors declare that there is no conflict of interest.

The author(s) disclosed receipt of the following financial support for the research, authorship, and/or publication of this article: This work was supported by the Aeronautical Corporation of China – Civil Aero Engine [contract number 126961]

References

1. Manjunath, R.N., Behera, B.K., and Mawkhlieng, U., Flexural stability analysis of composite panels reinforced with stiffener integral woven preforms. *The Journal of The Textile Institute*, 2018. **110**(3): p. 368-377.
2. Baucom, J.N. and Zikry, M.A., Low-velocity impact damage progression in woven E-glass composite systems. *Composites Part A: Applied Science and Manufacturing*, 2005. **36**(5): p. 658-664.
3. Yang, J.-M., Ma, C.-L., and Chou, T.-W., Fiber inclination model of three-dimensional textile structural composites. *Journal of composite Materials*, 1986. **20**(5): p. 472-484.
4. Whitney, T.J. and Chou, T.-W., Modeling of 3-D Angle-Interlock Textile Structural Composites. *Journal of Composite Materials*, 1989. **23**(9): p. 890-911.

5. Byun, J.H. and Chou, T.W., Elastic Properties of Three-dimensional Angle-interlock Fabric Preforms. *The Journal of The Textile Institute*, 1990. **81**(4): p. 538-548.
6. Adanur, S. and Liao, T.Y., 3D modeling of textile composite preforms. *Composites Part B-Engineering*, 1998. **29**(6): p. 787-793.
7. Chen, X. and Potiyaraj, P., CAD/CAM of orthogonal and angle-interlock woven structures for industrial applications. *Textile Research Journal*, 1999. **69**(9): p. 648-655.
8. Verpoest, I. and Lomov, S., Virtual textile composites software : Integration with micro-mechanical, permeability and structural analysis. *Composites Science and Technology*, 2005. **65**(15-16): p. 2563-2574.
9. Zeng, X.S., Brown, L.P., Endruweit, A., Matveev, M., and Long, A.C., Geometrical modelling of 3D woven reinforcements for polymer composites: Prediction of fabric permeability and composite mechanical properties. *Composites Part a-Applied Science and Manufacturing*, 2014. **56**: p. 150-160.
10. Boisse, P., Gasser, A., Hagege, B., and Billoet, J.-L., Analysis of the mechanical behavior of woven fibrous material using virtual tests at the unit cell level. *Journal of Materials Science*, 2005. **40**(22): p. 5955-5962.
11. Xu, M., Sitnikova, E., and Li, S., Unification and parameterisation of 2D and 3D weaves and the formulation of a unit cell for composites made of such preforms. *Composites Part A: Applied Science and Manufacturing*, 2020. **133**: p. 105868.
12. Li, S., Zhou, C., Yu, H., and Li, L., Formulation of a unit cell of a reduced size for plain weave textile composites. *Computational Materials Science*, 2011. **50**(5): p. 1770-1780.
13. Li, S. and Sitnikova, E., Representative volume elements and unit cells: concepts, theory, applications and implementation. 2019: Elsevier.
14. Li, S., Warrior, N., Zou, Z., and Almaskari, F., A unit cell for FE analysis of materials with the microstructure of a staggered pattern. *Composites Part a-Applied Science and Manufacturing*, 2011. **42**(7): p. 801-811.
15. Karahan, M., Lomov, S.V., Bogdanovich, A.E., Mungalov, D., and Verpoest, I., Internal geometry evaluation of non-crimp 3D orthogonal woven carbon fabric composite. *Composites Part A: Applied Science and Manufacturing*, 2010. **41**(9): p. 1301-1311.
16. Desplentere, F., Lomov, S.V., Woerdeman, D., Verpoest, I., Wevers, M., and Bogdanovich, A., Micro-CT characterization of variability in 3D textile architecture. *Composites Science and Technology*, 2005. **65**(13): p. 1920-1930.
17. Sitnikova, E., Xu, M., Kong, W., and Li, S., Controllable parameters as the essential components in the analysis, manufacturing and design of 3D woven composites. *Composites Science and Technology*, 2022. **230**: p. 109730.
18. Green, S.D., Matveev, M.Y., Long, A.C., Ivanov, D., and Hallett, S.R., Mechanical modelling of 3D woven composites considering realistic unit cell geometry. *Composite Structures*, 2014. **118**: p. 284-293.
19. Zhang, X., Zhang, S., Jia, Y., Liu, C., Gao, X., Wang, F., and Song, Y., A parameterized and automated modelling method for 3D orthogonal woven composite RVEs considering yarn geometry variations. *Composite Structures*, 2023. **305**: p. 116496.
20. Naouar, N., Vasiukov, D., Park, C.H., Lomov, S.V., and Boisse, P., Meso-FE modelling of textile composites and X-ray tomography. *Journal of Materials Science*, 2020. **55**(36): p. 16969-16989.
21. Isart, N., El Said, B., Ivanov, D.S., Hallett, S.R., Mayugo, J.A., and Blanco, N., Internal geometric modelling of 3D woven composites: A comparison between different approaches. *Composite Structures*, 2015. **132**: p. 1219-1230.
22. Wijaya, W., Ali, M.A., Umer, R., Khan, K.A., Kelly, P.A., and Bickerton, S., An automatic methodology to CT-scans of 2D woven textile fabrics to structured finite

- element and voxel meshes. *Composites Part A: Applied Science and Manufacturing*, 2019. **125**.
23. Liu, Y., Straumit, I., Vasiukov, D., Lomov, S.V., and Panier, S., Prediction of linear and non-linear behavior of 3D woven composite using mesoscopic voxel models reconstructed from X-ray micro-tomography. *Composite Structures*, 2017. **179**: p. 568-579.
 24. Mehdikhani, M., Gorbatikh, L., Verpoest, I., and Lomov, S.V., Voids in fiber-reinforced polymer composites: A review on their formation, characteristics, and effects on mechanical performance. *Journal of Composite Materials*, 2018. **53**(12): p. 1579-1669.
 25. Barburski, M., Straumit, I., Zhang, X., Wevers, M., and Lomov, S.V., Micro-CT analysis of internal structure of sheared textile composite reinforcement. *Composites Part A: Applied Science and Manufacturing*, 2015. **73**: p. 45-54.
 26. Wielhorski, Y., Mendoza, A., Rubino, M., and Roux, S., Numerical modeling of 3D woven composite reinforcements: A review. *Composites Part A: Applied Science and Manufacturing*, 2022. **154**.
 27. Kong, W., Macro-scale modelling of the impact response of 3D woven composites for aerospace applications. 2016, University of Nottingham.
 28. Lomov, S.V., Modeling the geometry of textile composite reinforcements: WiseTex, in *Composite Reinforcements for Optimum Performance*. 2021, Elsevier. p. 199-236.
 29. Lomov, S.V., WiseTex—A Virtual Textile Composites Software, in *Advanced Weaving Technology*. 2022, Springer. p. 293-318.
 30. Long, A.C. and Brown, L.P., 8 - Modelling the geometry of textile reinforcements for composites: TexGen, in *Composite Reinforcements for Optimum Performance*, P. Boisse, Editor. 2011, Woodhead Publishing. p. 239-264.
 31. Hivet, G. and Boisse, P., Consistent 3D geometrical model of fabric elementary cell. Application to a meshing preprocessor for 3D finite element analysis. *Finite elements in analysis and design*, 2005. **42**(1): p. 25-49.
 32. Wendling, A., Hivet, G., Vidal-Sallé, E., and Boisse, P., Consistent geometrical modelling of interlock fabrics. *Finite Elements in Analysis and Design*, 2014. **90**: p. 93-105.
 33. Li, S., Jeanmeure, L.F.C., and Pan, Q., A composite material characterisation tool: UnitCells. *Journal of Engineering Mathematics*, 2015. **95**(1): p. 279-293.
 34. Pan, Q., Multi-scale modelling and material characterisation of textile composites for aerospace applications. 2016, University of Nottingham.
 35. Abaqus/CAE User's Guide, Abaqus 2019 HTML Documentation. 2019.
 36. FAA, Composite Aircraft Structure, Federal Aviation Administration Advisory Circular, AC No:20-107B, Aug 2010, Change 1, F.A. Administration, Editor. 2010.
 37. Pierreux, G., Van Hemelrijck, D., and Massart, T.J., Automated generation of 3D orthogonal woven composites RVEs including yarn cross-section variations. *Composites Science and Technology*, 2019. **176**: p. 90-102.
 38. Soden, P., Hinton, M., and Kaddour, A., Lamina properties, lay-up configurations and loading conditions for a range of fibre reinforced composite laminates, in *Failure criteria in fibre-reinforced-polymer composites*. 2004, Elsevier. p. 30-51.